Dihydrosphingomyelin Impairs HIV-1 Infection by Rigidifying Liquid-Ordered Membrane Domains

Catarina R. Vieira,[1,7] Jose M. Munoz-Olaya,[2,7] Jesús Sot,[3,7] Sonia Jiménez-Baranda,[1] Nuria Izquierdo-Useros,[4] Jose Luis Abad,[2] Beatriz Apellániz,[3] Rafael Delgado,[5] Javier Martinez-Picado,[4,6] Alicia Alonso,[3] Josefina Casas,[2] José L. Nieva,[3] Gemma Fabriás,[2,8] Santos Mañes,[1,8,*] and Félix M. Goñi[3,8,*]

[1]Department of Immunology and Oncology, Centro Nacional de Biotecnología/CSIC, Darwin 3, E-28049 Madrid, Spain
[2]Department of Biomedicinal Chemistry, Institute of Advanced Chemistry of Catalonia (IQAC)/CSIC, Jordi Girona 18, 08034 Barcelona, Spain
[3]Unidad de Biofísica (Centro Mixto CSIC-UPV/EHU) and Departamento de Bioquímica, Universidad del País Vasco, P.O. Box 644, E-48080 Bilbao, Spain
[4]irsiCaixa Foundation, Hospital Universitari Germans Trias i Pujol, E-08916 Badalona, Spain
[5]Hospital Universitario 12 de Octubre, Avenida. Andalucía s/n, E-28049 Madrid, Spain
[6]ICREA, Barcelona, Spain
[7]These authors contributed equally to this work
[8]These authors contributed equally to the design and direction of this work
*Correspondence: felix.goni@ehu.es (F.M.G.), smanes@cnb.csic.es (S.M.)
DOI 10.1016/j.chembiol.2010.05.023

SUMMARY

The lateral organization of lipids in cell membranes is thought to regulate numerous cell processes. Most studies focus on the coexistence of two fluid phases, the liquid crystalline (l_d) and the liquid-ordered (l_o); the putative presence of gel domains (s_o) is not usually taken into account. We show that in phospholipid:sphingolipid:cholesterol mixtures, in which sphingomyelin (SM) promoted fluid l_o domains, dihydrosphingomyelin (DHSM) tended to form rigid domains. Genetic and pharmacological blockade of the dihydroceramide desaturase (Des1), which replaced SM with DHSM in cultured cells, inhibited cell infection by replication-competent and -deficient HIV-1. Increased DHSM levels gave rise to more rigid membranes, resistant to the insertion of the gp41 fusion peptide, thus inhibiting viral-cell membrane fusion. These results clarify the function of dihydrosphingolipids in biological membranes and identify Des1 as a potential target in HIV-1 infection.

INTRODUCTION

Biological membranes show lateral heterogeneity due to the presence of lipid domains (Mukherjee and Maxfield, 2004), which is proposed to be central to cell physiology by spatially and temporally regulating the formation of multimolecular complexes at the cell surface (Goñi et al., 2008). Identification of factors that regulate phase formation in living cells would thus be relevant in pathophysiological processes, including cell infection by many intracellular pathogens (Mañes et al., 2003).

Two lamellar phases have been classically defined in model membranes: the gel or solid-ordered (s_o) and the liquid-crystalline or disordered (l_d) phase. Saturated and unsaturated phospholipids partition preferentially into the s_o and l_d phases,

respectively. A liquid-ordered (l_o) phase has also been described in the presence of cholesterol (Chol) (Ipsen et al., 1987). In the l_o phase, acyl chains are in a highly ordered conformation but lateral lipid diffusion is allowed. The so-called lipid rafts, enriched in sphingomyelin (SM) and Chol, appear to exist in the l_o phase (Edidin, 2003).

A variety of physical techniques applied to liposomes containing mixtures of SM:PC (phosphatidylcholine) and/or Chol have shown the coexistence of gel and fluid, gel and l_o, and l_o and l_d domains (Almeida et al., 1993; Collado et al., 2005). Coexistence of the three s_o, l_o and l_d phases has been visualized directly in giant unilamellar vesicles (GUV) containing SM:PC: Chol:Ceramide (Cer) and SM:PC:PE (phosphatidylethanolamine):Chol (Chiantia et al., 2006; de Almeida et al., 2007; Sot et al., 2008). Segregation of l_o- and l_d-like domains in the micrometer range is reported for vesicles isolated from the plasma membrane of cultured mammalian cells (Baumgart et al., 2007). Fluorescence recovery after photobleaching (FRAP) studies indicated the coexistence of l_o and l_d phases in the plasma membrane of epithelial cells (Meder et al., 2006), suggesting that the same self-organizing principles operate in model and in living cell membranes. Others found a wide spectrum of lipid domains with different physical properties in the live cell plasma membrane, suggesting submicroscopic, unstable l_o-like domains on the cell surface (Hancock, 2006; Jacobson et al., 2007; Kusumi et al., 2004; Sharma et al., 2004).

Study of phase formation in living cells has been hampered by the diversity of lipid species in the plasma membrane. Biological studies have shown the segregation of different sphingolipid species in distinct regions of the plasma membrane of polarized cells (Brugger et al., 2004; Fujita et al., 2007; Gómez-Moutón et al., 2001). To add further complexity, cell membranes contain "unusual" sphingolipids, such as dihydrosphingomyelins (DHSM), whose biophysical properties have not been studied in detail. Glycosphingolipids and SM are produced from Cer, which is in turn biosynthesized de novo in four steps from serine and palmitoyl-CoA (Kolter and Sandhoff, 2006). The final reaction is the introduction of the (E)-4 double bond into the sphinganine backbone by the dihydroceramide desaturases Des1 and

Des2. Inhibition of Des1 and/or Des2 should lead to an increase in DHSM while reducing SM levels.

Dihydrosphingolipid levels are not high in cells, except for the unusual DHSM enrichment in the human lens (Byrdwell et al., 1994), and in the human immunodeficiency virus (HIV)-1 envelope (Brugger et al., 2006; Lorizate et al., 2009). Biophysical studies of liposomes showed that DHSM interacts with higher affinity than acyl-chain-matched SM with Chol and increases stability and packing of model membranes (Kuikka et al., 2001); this observation is further confirmed by comparison of the rate and extent of cholesterol crystallite formation with SM and DHSM (Epand, 2003). Nonetheless, the relevance of DHSM in domain formation or membrane fluidity has not been shown in living cells.

We explored the functional effects of replacing SM with DHSM in artificial membranes and in cell plasma membranes. Domain formation was studied in GUV containing different amounts of SM and DHSM, in addition to PC, PE, and Chol. SM was replaced with DHSM in plasma membrane by cell incubation with two Des1 inhibitors (Triola et al., 2004). To analyze the biological relevance of DHSM in live cells, we determined the effect of Des1 inhibitors on HIV-1 infection of susceptible cells as a paradigm of a lipid phase-regulated process.

RESULTS

DHSM Rigidifies I_o Domains in GUV Formed By Ternary Mixtures

Studies in artificial membranes support the idea that DHSM-containing liposomes form with Chol more condensed I_o domains than those containing SM (Kuikka et al., 2001; Nyholm et al., 2003a, 2003b; Ollila and Slotte, 2002). To address the role of DHSM in biological membranes, we initially studied the generalized polarization (GP) of Laurdan in bilayers formed by SM, DHSM, and Chol. A decrease in Laurdan GP is directly related to an increase in water access to the interface and an indication of increased bilayer fluidity (Parasassi et al., 1990). As predicted, DHSM:Chol bilayers showed higher Laurdan GP values than those consisting of SM:Chol in the 15°C–50°C temperature range (Figure 1A); temperature increase fluidified the bilayer and GP decreased accordingly. SM replacement with different amounts of acyl-matched DHSM promoted a dose-dependent increase in GP values at all temperatures tested (Figure 1A), indicating rigidification of the bilayer.

GUV composed of PC:PE:Chol and SM or DHSM were stained with the fluorescent probes DiI and NBD-Cer. DiI partitions preferentially in I_d domains, whereas the NBD-Cer probe binds similarly to I_o and I_d domains, but is excluded from s_o phases (Sot et al., 2008). The DiI probe stained PC:PE:SM:Chol and PC:PE:DHSM:Chol vesicles similarly, indicating that DHSM did not alter I_d phase formation (Figure 1B). Since a change in bilayer composition could change DiI partitioning into the I_d/I_o domains (Bagatolli, 2006), control experiments using the I_o phase probe Laurdan confirmed that DiI specifically stained I_d domains in both lipid mixtures (not shown). In contrast, NBD-Cer stained PC:PE:DHSM:Chol GUV more weakly compared to PC:PE:SM:Chol GUV (Figure 1B). This reduction in NBD-Cer staining was evident in the region from which DiI was excluded. Indeed, the ratio of NBD-Cer fluorescence intensity in the I_o to the I_d phases

was clearly lower in DHSM-containing GUV (SM-GUV: 1.06 ± 0.16; DHSM-GUV: 0.42 ± 0.13; Figure 1C). This suggests the presence of s_o phase domains interspersed in the I_o phase of PC:PE:DHSM:Chol bilayers. Three-dimensional reconstructions of DHSM-GUV show two main domains, circular in shape, limiting one I_d and one I_o macrodomain (see Figure S1 available online). Circular boundaries are an indication of liquid-liquid domain coexistence (Bagatolli, 2006). This supports our previous assertion that there is not a single, macroscopically separated s_o domain, but rather a number of s_o microdomains interspersed within the I_o phase.

The presence of rigid, gel-like domains in bilayers containing DHSM was further studied using di-4-ANEPPDHQ. Emission fluorescence of this probe shifts toward red when inserted in I_d and toward green when incorporated in I_o environments (Jin et al., 2006). Confocal analysis of SM-containing GUV showed regions predominantly in the I_d phase (yellow in merge image) mixed with smaller I_o domains (green). In contrast, we observed substantial unstained areas in DHSM-containing vesicles, suggesting the presence of more rigid domains (Figure 1D). Quantification of emission spectra showed a notable reduction in the area below the I_o spectrum of DHSM- compared with SM-containing GUV; however, I_d spectra were comparable in both (Figures 1E and 1F). The results suggest that DHSM-induced s_o domains are formed essentially at the expense of the I_o phase (Sot et al., 2008).

Differential scanning calorimetry (DSC) data decisively supported the presence of gel domains in DHSM-containing bilayers. When a gel phase melts cooperatively into a fluid domain, a DSC endotherm is observed, whereas I_o-I_d thermal transitions are not detected. We found a clear endotherm extending from 20°C to 50°C in DHSM- but not in SM-containing GUV, indicating gel domain melting under these conditions (Figure 1G). In summary, our results indicate that DHSM in the bilayer imposes a change from fluid I_o to s_o domains. This is in agreement with previous observations of a rigidifying effect of DHSM, although evidence of s_o domain formation was lacking.

Chemical Inhibition of Des1 Increases DHSM Levels in I_o Domains of Living Cells

Since replacement of only 30% of SM by DHSM induced a clear change in bilayer rigidity (Figure 1A), we analyzed the effect of increasing DHSM levels in the plasma membrane of living cells. Inhibition of Des1, the main enzyme introducing unsaturation into dihydroceramides (DHCer), seemed an attractive means of increasing DHSM levels in cultured cells. The compound GT11 effectively inhibits Des1 activity in neurons (Triola et al., 2004). Toxicity studies in HEK293 cells indicated that 24 hr incubation with GT11pyr (a hydrophilic derivative of GT11; Figure 2A) at concentrations ≤30 μM minimally affected cell growth (Figure 2B). Cell cycle analyses indicated a dose-dependent increase in the percentage of GT11pyr-treated cells in the S-phase peak, with a concomitant decrease in the G2/M peak (Figure 2C). At the doses tested, GT11pyr did not affect the subG0/G1 peak compared with controls (Figure 2C). Short incubation (≤24 hr) with GT11pyr does not cause cell death, although it might slow cell cycle progression.

We compared the relative potency of GT11pyr and GT11 in inhibiting Des1 activity. Lysates of HEK293 cells and TZM-b1,
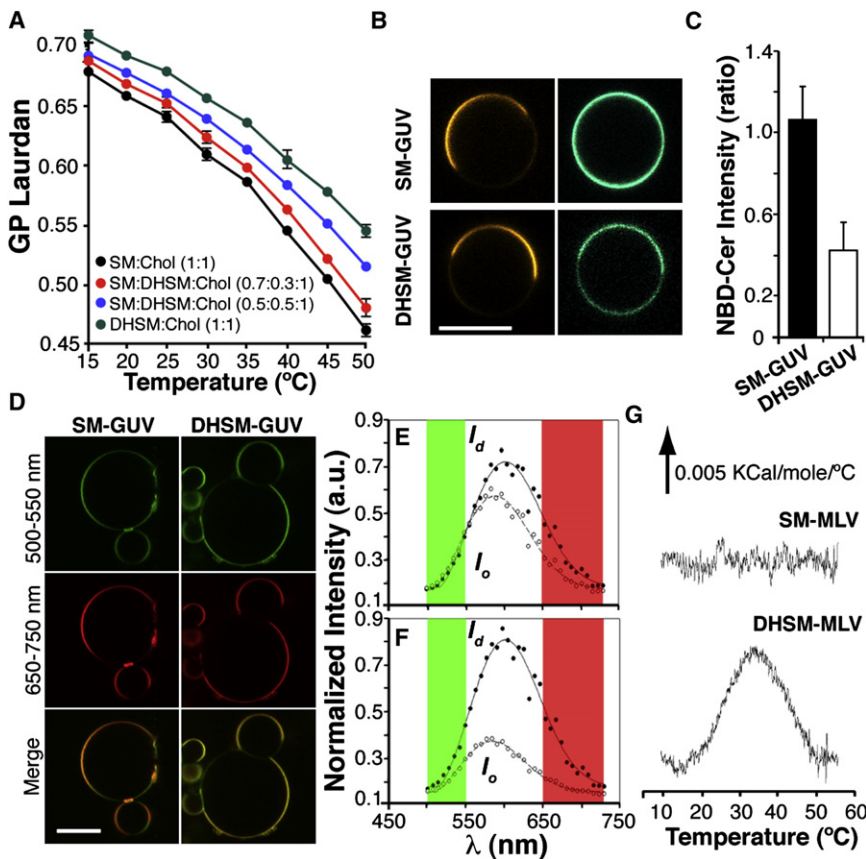
Figure 1. DHSM Forms Gel-Like Domains in GUV

(A) Temperature variation of the GP of Laurdan embedded in phospholipid bilayers with indicated lipid compositions. Mean values ± SEM are shown (n = 3); in some cases, error bars are smaller than symbol size.

(B) Representative confocal images (equatorial sections) of PC:PE:SM:Chol and PC:PE:DHSM:Chol GUV (1:1:1:1, mol ratio) stained with NBD-Cer (left) and DiI probes (right). Bar = 10 µm.

(C) Ratio of NBD-Cer fluorescence intensity measured in the DiI dark to bright regions of SM- and DHSM-GUV as in (B). Mean values ± SEM (n = 12).

(D) Representative confocal images (equatorial section) showing di-4-ANEPPDHQ probe distribution in I_o and I_d fluid domains of PC:PE:SM:Chol and PC:PE:DHSM:Chol GUV. Individual channels and merge images are shown. Bar = 10 µm.

(E and F) Emission spectra from I_o and I_d domains of PC:PE:SM:Chol (E) PC:PE:DHSM:Chol (F) GUV, represented as normalized fluorescence intensity at the different wavelengths.

(G) DSC thermograms of the quaternary lipid mixtures (PC:PE:Chol:SM or DHSM, 1:1:1:1 mol ratio) dispersed in the form of MLV. The endotherm observed with the DHSM-MLV corresponds to a thermotropic phase transition with ΔH = 0.49 kcal/mol DHSM. See also Figure S1.

a CD4- and CCR5-expressing HeLa subclone, were incubated with different amounts of GT11 and GT11pyr, and Des1 activity determined by HPLC using DHCerC6NBD as substrate (Munoz-Olaya et al., 2008). GT11 and GT11pyr inhibited Des1 activity in a dose-dependent manner with similar potency (Figure 2D).

To determine whether Des1 inhibition leads to effective replacement of SM by DHSM in the cell membrane, we isolated sphingolipid-enriched detergent-resistant membrane (DRM) fractions from HEK293 cells, untreated or treated with GT11pyr for 24 hr, and analyzed lipid composition by ultra performance liquid chromatography (UPLC) coupled to mass spectrometry, using C16 SM as a probe (the most abundant SM in this cell type). Representative chromatograms of vehicle and GT11pyr (30 µM)-treated cells are shown (Figure 2E). GT11pyr promoted a dose-dependent decrease in the relative amount of C16 SM, which paralleled an increase in the amount of DHSM species in the DRM fraction (Figure 2F). The DHSM/SM ratio reached a maximum of 0.3 at 30 µM GT11pyr (Figure 2F). We found comparable variation in the DHSM/SM ratio for C16:0, C24:0, and C24:1 species after GT11pyr treatment (Table S1). GT11pyr also increased the amount of DHCer while decreasing Cer levels in DRM in a dose-dependent manner (Table S2); nevertheless, Des1 inhibition affected neither glucosylceramide or lactosylceramide levels nor the SM/glycosphingolipid ratio (Figure S2). These results indicate that GT11pyr-induced inhibition of Des1 causes the partial replacement of SM and Cer by DHSM and DHCer in living cells. It should nonetheless be noted that Cer and DHCer levels are much lower than those for SM and DHSM in this cell type.

Increased DHSM Levels Inhibit HIV-1 Infection

We used HIV-1 infection as a model to study the consequences of the increase in cellular DHSM. HIV-1 infection entails sequential interactions between the viral envelope (Env) gp120 subunit with CD4 and to obligate coreceptors (usually CCR5 or CXCR4), which enables refolding of the Env gp41 fusogenic subunit, followed by viral and cell membrane fusion. Fusion efficiency is controlled by the clustering of CD4-gp120-coreceptor complexes at the cell surface (Kuhmann et al., 2000) and by insertion of the fusion peptide into the host cell membrane. The actin cytoskeleton (Barrero-Villar et al., 2009; Jimenez-Baranda et al., 2007; Jolly et al., 2004) and host cell membrane lipid composition are key determinants for efficient infection. Indeed, cholesterol sequestration or inhibition of sphingolipid biosynthesis attenuates virus entry into T cells, monocytes, and cell lines engineered to express HIV-1 receptors (Mañes et al., 2000; Hug et al., 2000; Liu et al., 2002; Carter et al., 2009).

To analyze whether decreasing Des1 activity affects HIV-1 infection of target cells, we incubated TZM-b1 cells with subtoxic doses of GT11pyr (15–30 µM), followed by exposure to equal amounts of replication-deficient pNL4.3lucR-E viruses (He et al., 1995) pseudotyped with ADA (R5 strain), NL4.3 (X4 strain), or vesicular stomatitis virus (VSV)-G (control) envelopes.
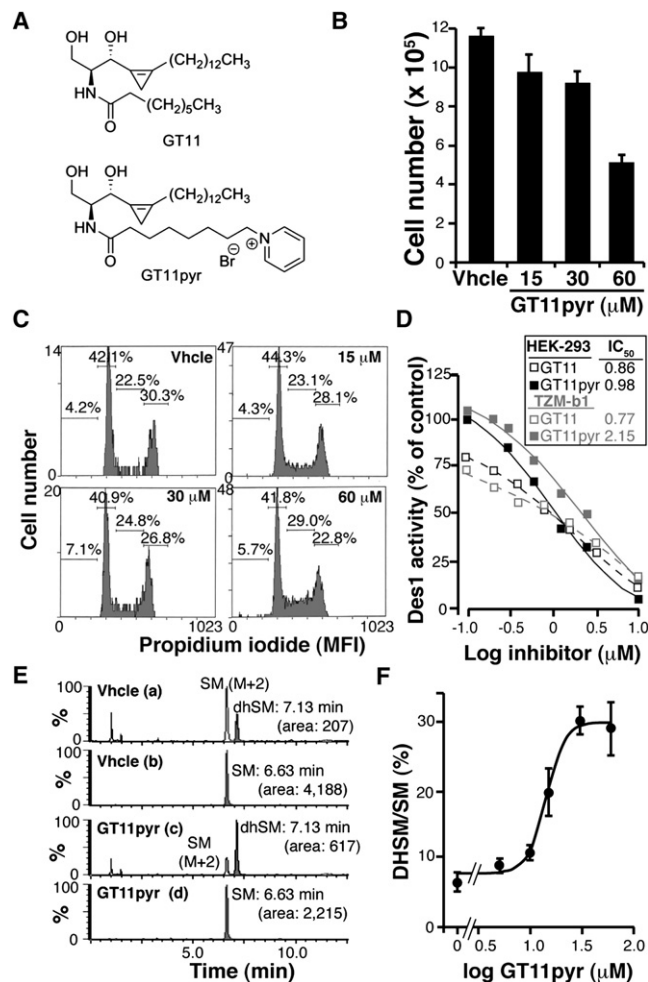
Figure 2. Des1 Inhibition Replaces SM with DHSM in Cell Membranes

(A) Chemical structure of the GT11 and GT11pyr inhibitors used.

(B) Effect of GT11pyr doses indicated on viable HEK293 cell number determined by trypan blue exclusion; determinations were performed by triplicate for each condition (n = 3).

(C) Effect of GT11pyr on cell cycling determined by propidium iodide. A representative of three experiments is shown.

(D) GT11 (open symbols) and GT11pyr (solid symbols) inhibition of Des1 activity in whole cell lysates of HEK293 (black) and TMZ-b1 (red) using DHCer6-NBD as substrate.

(E) Representative chromatograms obtained by selecting the exact masses of C16-SM $[(SM+H)^+$: 703.5749 amu; chromatograms b, d] and C16-DHSM $[(DHSM+H)^+$: 705.5911 amu; chromatograms a, c] in data acquired with UPLC/TOF from lipid extracts of vehicle- (chromatograms a, b) or GT11pyr-treated cells (chromatograms c, d). Retention times (min) and peak areas are indicated.

(F) GT11pyr-induced dose-dependent changes in the DHSM/SM ratio calculated from chromatograms in (B). Data are the mean ± SD of three replicates. See also Tables S1 and S2, and Figure S2.

GT11pyr reduced cell infection by ADA- and NL4.3-pseudotyped viruses up to 60%, without affecting entry of VSV-G virions (Figure 3A). Since VSV-G-pseudotyped viruses effectively infected GT11pyr-treated cells, the inhibitory effect of this compound is HIV Env-specific and is not due to a cytotoxic effect. Independent infection experiments using the replica-
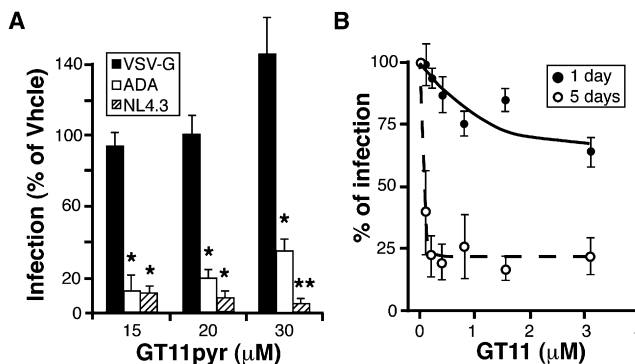

Figure 3. Increased DHSM Levels by Des1 Inhibition Reduces HIV-1 Infection

(A) TZM-b1 cells pretreated with indicated GT11pyr doses (24 hr) were exposed to luciferase (luc)-encoding HIV-1 viruses pseudotyped with R5, X4, and VSV-G envelopes. Luc activity was recorded to quantify cell infection.

(B) TZM-bl cells were incubated with GT11 (0.1–3 μM) for 24 hr (solid symbols) or 5 days (open symbols) and then infected with replication-competent HIV-1$_{NFN-SX}$ viruses. Cells were assayed for luciferase activity 48 hr later. Values indicate mean ± SEM of a representative experiment. *p ≤ 0.02, **p ≤ 0.001 unpaired Student's t test.

tion-competent HIV-1$_{NFN-SX}$ strain in TZM-b1 cells treated with the hydrophobic inhibitor GT11 showed a time- and dose-dependent inhibitory effect on HIV-1 infection (Figure 3B) at nontoxic GT11 doses (not shown). The time-dependent inhibitory effect at very low GT11 doses might reflect slow replacement of SM by DHSM at suboptimal inhibitory concentrations of Des1, although possible "long-term" pleiotropic effects of the compound cannot be ruled out. These results indicate that GT11 and GT11pyr specifically inhibit cell infection by X4- and R5 HIV-1 strains.

To confirm a role for Des1 in HIV-1 infection, we analyzed virus infectivity in TZM-b1 cells transfected with Des1-specific small interference (si)RNA. Knockdown of Des1 reduced Des1 protein levels (Figure 4A) and activity (Figure 4B) without affecting cell viability (Figure S3); Des1 silencing also increased the DHCer/Cer ratio (35%–40%) compared with mock- (2%–4%) or mismatched siRNA-transfected cells (5%–12%). HIV-1$_{NFN-SX}$ infection (10 ng p24) in TZM-b1 cells transfected with Des1-specific siRNA was significantly reduced compared to mock- or mismatched siRNA-transfected cells (Figure 4C). Similar inhibition of infection was observed at higher (50 ng) and lower (2 ng) viral doses (Figure S4). Pharmacological and genetic interference with Des1 activity thus inhibited HIV-1 infection of target cells.

Increased DHSM Levels Do Not Affect HIV-1 Receptor Clustering

Previous reports indicate that gp120-induced receptor clustering is sensitive to lipid modulation. Cholesterol depletion prevents gp120 triggering of CD4-coreceptor colocalization (Mañes et al., 2000) and decreases CCR5 diffusion (Steffens and Hope, 2004). Cell treatment with acid sphingomyelinase (SMase), which transforms SM to Cer, also restricts lateral CD4 mobility (Finnegan et al., 2004, 2007). Ceramides tend to form s_o domains in artificial membranes (Cremesti et al., 2002; Megha, 2004);
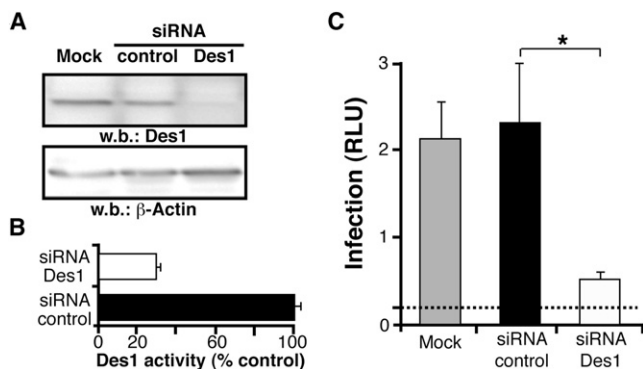
Figure 4. Des1 Silencing Inhibits HIV-1 Infection

(A) TZM-bl cells were transfected with vehicle (mock), mismatched, or Des1-specific siRNA; after 4 days, Des1 protein levels were analyzed in cell extracts (20 μg/lane). The same membranes were probed with an anti-β-actin antibody as loading control. A representative experiment is shown (n = 3).

(B) Des1 activity was assayed in total cell extracts of TZM-b1 cells as in (A), using DHCer6-NBD as substrate.

(C) The same cells as in (A) were pulsed with HIV-1$_{NFN-SX}$ virus (10 ng p24) and infectivity recorded by luciferase activity; each point represents the mean ± SEM of four replicates (n = 2). *p ≤ 0.02 unpaired Student's t test. See also Figures S3 and S4.

since DHSM also rigidifies lipid bilayers, GT11pyr-induced inhibition of HIV-1 infection might be explained by impaired clustering of viral receptors.

Analysis of the protein composition of the same DRM fractions in which the maximal DHSM/SM ratio was detected (Figure 2F) showed no differences in CD4 partitioning between DRM and soluble fractions in vehicle- and GT11pyr-treated cells (Figure 5A). Des1 inhibition did not alter the unique partitioning of either caveolin or the transferrin receptor, used as controls for DRM-associated and -excluded membrane proteins, respectively (Figure 5A). There were also no differences between vehicle- and GT11pyr-treated cells in colocalization of CD4 and CXCR4 HIV-1 receptors with ganglioside GM1 (Figure 5B).

We analyzed the effect of GT11pyr on the formation of higher order molecular complexes between gp120, CD4, and CXCR4. Receptor overexpression is reported to overcome the lipid-modulatory effect of gp120-induced CD4 and/or coreceptor clustering (Finnegan et al., 2007; Viard et al., 2002). To avoid misleading effects due to receptor overexpression, we used resting peripheral blood mononuclear cells (PBMCs) in coclustering experiments; assays were carried out at 12°C to avoid receptor internalization. gp120 induced formation of large CD4- and CXCR4-containing clusters (Figure 5C), which did not differ in number or size in vehicle- or GT11pyr-treated PBMCs (Figures 5D and 5E). The results suggest that the adverse effect of GT11pyr in HIV-1 infection is not a result of impaired lateral mobility of HIV-1 receptors.

DHSM-Induced Rigidification Inhibits gp41 Insertion and Fusion

The effect of Des1 inhibitors on HIV-1 infection might alternatively be explained by regulation of gp41-mediated fusion of viral and cell membranes. Vesicle fusion involves the formation of nonlamellar intermediates with inverted phase structure

(Goñi and Alonso, 2000); indeed, the gp41 fusion peptide lowers the hexagonal phase transition temperature (T_H) after insertion in bilayers (Peisajovich et al., 2000), enabling the formation of inverted-hexagonal structures. DHSM stabilizes the lamellar phase toward the inverted hexagonal phase, but no more so than SM (Figure S5); lamellar phase stabilization by DHSM thus cannot explain any inhibitory effect on HIV-1 fusion.

Lipids could nonetheless impair the interaction between HIV-1 gp41 and the host cell membrane. SM and Chol promote surface aggregation of the gp41 pretransmembrane sequence (LWYIK) into l_o membranes (Saez-Cirion et al., 2002). To study whether the DHSM-imposed change in physical properties of the bilayer prevented fusion peptide insertion, we used intervesicular lipid mixing to quantitate fusion of large unilamellar vesicles (LUV) induced by the pretransmembrane stretch of gp41 (HIVc). DHSM in the LUV greatly decreased the extent of HIVc-induced intervesicular fusion at 25°C (Figure 6A); this inhibitory effect was lost at temperatures that induce melting of s_o domains (50°C) (Figures 1F and 6A, inset). The results indicate that gp41 fusion peptide insertion is impaired in membranes with high DHSM levels at temperatures at which s_o domains are present. We next analyzed gp160-induced cell-cell fusion in GT11-treated cells. Only HEK293-CD4 target cells were treated with the compound (24 hr), which was removed before coincubation with HEK293-gp160 cells. We observed dose-dependent inhibition of gp160-induced cell-cell fusion in GT11-treated cells (Figure 6B). Together, these results suggest that blockade of Des1 activity inhibits HIV-1 infection by decreasing gp41 insertion into the rigidified microdomains formed by the concurrent increase in DHSM levels.

DISCUSSION

The lateral organization of lipids in the plasma membrane is proposed to be central to cell physiology and is thought to be co-opted by many intracellular pathogens for cell infection (Mañes et al., 2003). The concept that HIV-1 hijacks lipid microdomains in the membrane for infection has been studied extensively (Mañes et al., 2000; Hug et al., 2000; Liao et al., 2001; Gallo et al., 2003). Most evidence is based on drastic cell treatments that, rather than affecting specific microdomains, destroy the general organization of the membrane. Moreover, these treatments involve the elimination of lipid species, raising the question whether the inhibition of HIV-1 infection is due to perturbation of membrane phases or to the requirement for such lipids for virus entry.

We designed a strategy to define the contribution of microdomain physical properties to the HIV-1 infectivity process by targeting Des1. Des1 inhibition impedes double bond formation in sphingolipids, thus increasing the presence of otherwise rare dihydrosphingolipids. This can alter the physical properties of the bilayer without eliminating sphingolipid species. Our biophysical studies establish that in lipid bilayers, DHSM induces formation of gel-like domains interspersed in the l_o phase. In cells, increasing amounts of DHSM, induced by cell treatment with two Des1 inhibitors or by knock-down of Des1 expression, correlated with lower cell susceptibility to HIV-1 infection and Env-mediated cell-cell fusion. We predict that the DHSM increase in the membrane of Des-1-inhibited cells fosters the
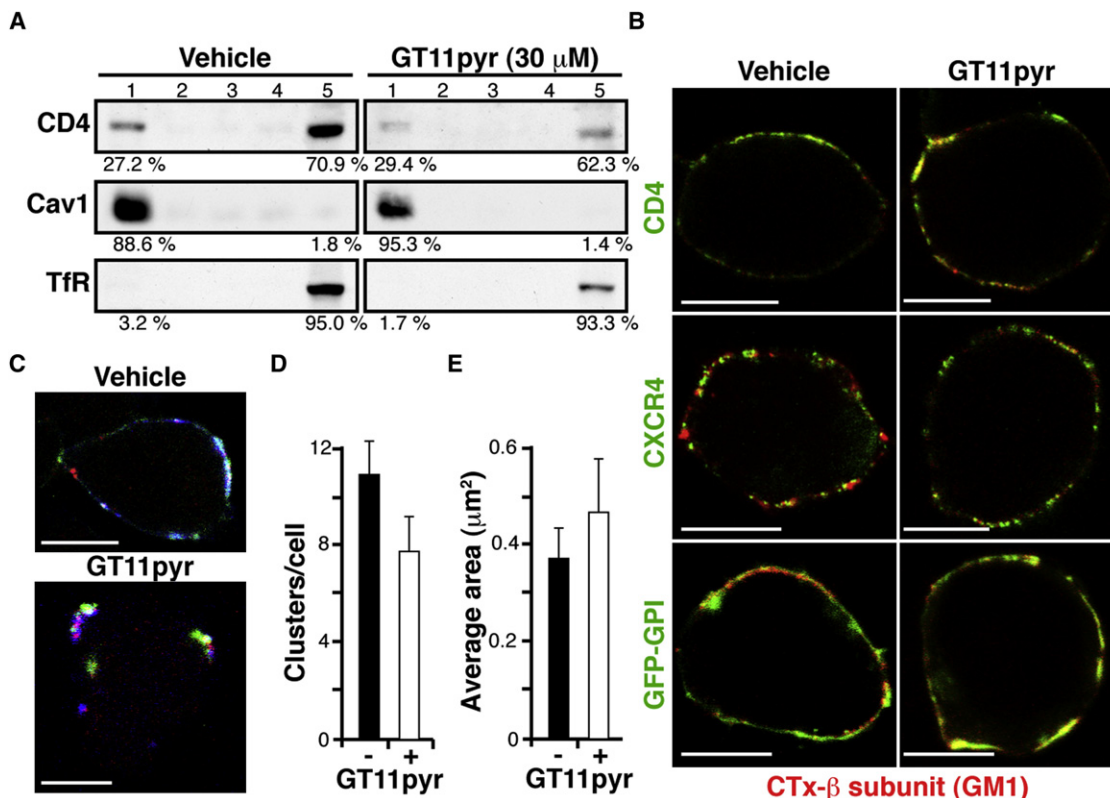
Figure 5. GT11pyr Treatment Does Not Affect HIV-1 Receptor Clustering

(A) The same gradient fractions used in Figure 2E were analyzed in immunoblot with the indicated antibodies. The relative abundance of the proteins in DRM (lane 1) and soluble (lane 5) fractions is indicated. A representative experiment is shown (n = 3).

(B) Colocalization of CD4, CXCR4, and GFP-GPI (all stained in green) after antibody-induced copatching (12°C) with the cholera toxin (CTx)-β subunit (red) in HEK293 cells. Representative merged images are shown (n = 15 for each protein).

(C–E) Antibody induced coclustering of gp120Env IIIB (X4 strain, red) with CD4 (green) and CXCR4 (blue) in PBMCs. Representative cells are shown (C, n = 10). Images were processed with ImageJ particle analyzer to determine the number (D) and area (E) of the clusters formed. Bar = 5 μm.

creation of rigid microdomains in which insertion of the gp41 fusion peptide is less efficient than in untreated cells; this in turn impairs viral-host cell membrane fusion and HIV-1 infection (Figure 7). Although our results in model membranes provide a mechanistic explanation of the reduced HIV-1 infection observed in Des1-inhibited cells, whether a DHSM increase also promotes formation of s_o-like domains in cells needs further research.

Although the existence of s_o phases in pure lipid bilayers has been known for decades (Luzzati et al., 1968), only recently has their presence been reported in cell membranes in physiological conditions, particularly in the presence of Cer (Goñi and Alonso, 2009; Taniguchi et al., 2006; Zhang et al., 2009). We propose that DHSM also gives rise to gel domains in the presence of other phospholipids and of sterols. Some of our fluorescence spectroscopy data could be interpreted in terms of formation of bi- or trimolecular complexes, e.g., DHSM/Chol or DHSM/(Chol)$_2$, which would mix with other lipid molecules without giving rise to a separate phase. The DSC calorimetric data can nonetheless originate only from domains with a minimum critical size, typically a few thousand molecules, able to produce a cooperative phase transition (Mabrey and Sturtevant, 1976). Our DSC data (Figure 1G) can thus be explained

only in terms of gel domains coexisting with fluid domains. The precise composition of these domains cannot be ascertained at present, but the fact that they are observed in a complex mixture (PC/PE/SM or DHSM/Chol) that contains the four major lipids found in cell membranes supports the idea that similar gel domains can form in Des-1-inhibited cells. That DHSM actually forms gel domains in membranes, rather than rendering them uniformly more rigid, is supported by the inhibition of gp41 fusion peptide insertion in lipid bilayers in the presence of DHSM at 25°C but not at 50°C, a temperature above the melting point of the gel domains. The SM and DHSM used here contain mainly palmitic acid (C16:0). The physical properties of gel phases formed by natural SM mixtures in cell membranes might be somewhat different. Saturated C16 to C24 SM, by far the most abundant in mammals, all have gel-fluid transition temperatures from 41°C–57°C (http://www.lipidat.tcd.ie), equal to or above the transition temperature of egg SM. Mammalian DHSM will thus form gel domains more easily than the egg derivative.

Although cell treatment with GT11pyr altered the DHSM/SM ratio in DRM by a maximum of 30% (Figure 2F), this level of SM:DHSM replacement in GUV was sufficient to modify bilayer rigidity as detected by GP of Laurdan (Figure 1A). Despite the physical changes imposed by DHSM, we found no difference
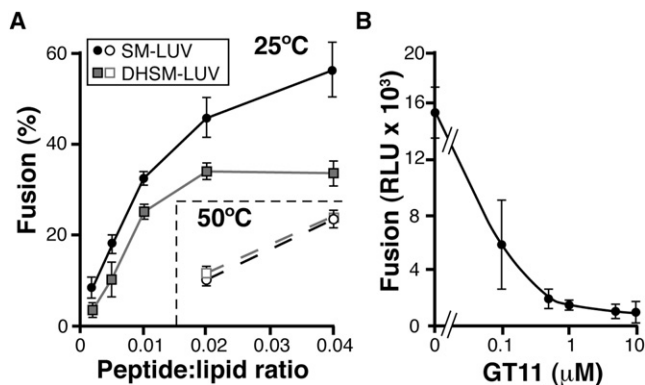
Figure 6. gp41 Insertion Is Impaired in DHSM-Rich Membranes

(A) HIVc-induced fusion of PC:PE:Chol:SM or DHSM (1:1:1:1 mol ratio) LUV. Intervesicular lipid mixing is shown as a function of the peptide-to-lipid ratio at 25°C (solid symbols and line) and 50°C (open symbols, dashed lines). Data points are the increase in NBD fluorescence (% after 30 min) measured at 530 nm (excitation at 465 nm) with a cutoff filter at 515 nm. Lipid concentration in all assays was 100 μM.

(B) HEK293-CD4 target cells were pretreated with GT11 at the indicated concentrations before coculture with gp160IIIB-expressing effector cells. Cell-cell fusion was quantified by measurement of luc activity in cell lysates. Values are mean ± SEM of triplicates in one representative experiment (n = 4). See also Figure S5.

in the gp120-induced lateral motility of CD4 and CXCR4 between vehicle- and GT11pyr-treated cells (Figures 5C–5E). This contrasts with reports on sphingomyelinase-treated cells, in which increased Cer levels reduced CD4 diffusion (Finnegan et al., 2007). The difference might be due to the far greater rigidifying effects of Cer compared with those of SM or DHSM (Sot et al., 2006, 2008). Indeed, our results suggest differences in the way that Cer and DHSM mix with SM-rich l_o domains. Confocal microscopy of GUV shows that Cer gives rise to micrometer-size gel domains, whereas DHSM-induced s_o domains are much smaller. These latter domains are poorly resolved by fluorescent confocal microscopy (compare Figure 6 in Sot et al., 2008, and our Figures 1B and 1C), although DSC unequivocally demonstrates the presence of gel domains in DHSM-containing samples (Figure 1F). DHSM domains might not affect the behavior of neighboring l_o regions into which HIV-1 receptors partition. Indeed, Des1 inhibitors had no effect on T cell activation and chemotaxis (Figure S6), two processes in which l_o domains play a critical role (Mañes and Viola, 2006).

In summary, our biophysical and biological evidence shows that DHSM forms lipid domains different from and more rigid than SM-rich l_o phases. DHSM-, Chol-rich domains might exist in a gel-like form in cell membranes. Inhibition of gp41-mediated fusion simply by replacing a minor fraction of sphingolipids with dihydrosphingolipids clearly demonstrates how membrane phase segregation controls pathophysiological processes in living cells.

SIGNIFICANCE

The plasma membrane is widely recognized as a heterogeneous cell compartment, given the coexistence of several kinds of lipid microdomains. HIV-1 co-opts the lateral orga-
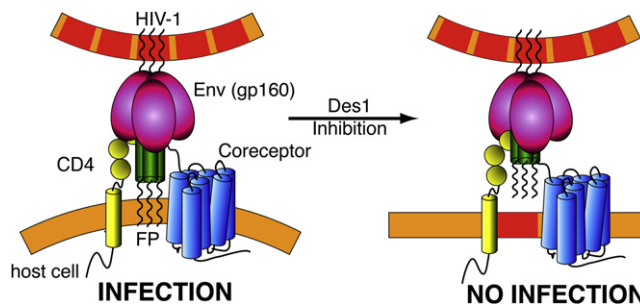

Figure 7. Proposed Model for the Blockade of HIV-1 Entry by Des1 Inhibition

In untreated cells, in which DHSM levels are low, gp120-induced clustering of CD4 and the coreceptors enables insertion of the gp41 fusion peptide (FP) into the cell membrane (left). Des1 inhibition increases DHSM levels, creating rigid microdomains (red areas) interspersed in the l_o phase (orange); gp41 insertion into DHSM domains is impaired, which attenuates virus entry (right).

nization of the plasma membrane to accumulate receptors and lipids in those regions in which host-viral membrane fusion will occur. This "intelligent" infection strategy used by HIV-1 can also be its Achilles' heel, however, as it can be used to interfere with virus entry into the cell. Here we explored the consequences of targeting dihydroceramide desaturase (Des)1 in HIV-1 infection. Des1 inhibition effectively replaced sphingolipids with dihydrosphingolipids in the membrane of cultured cells and inhibited HIV-1 cell infection. Dihydrosphingomyelin (DHSM), the most abundant dihydrosphingolipid in our cell lines, induces formation of rigid gel-like domains interspersed in the liquid-ordered phase of model membranes. As a consequence of DHSM accumulation, membrane microdomains are formed with sufficient rigidity to hinder gp41 fusion peptide insertion. Despite the membrane rigidity imposed by dihydrosphingolipids, we found no alteration in gp120-induced lateral motility of CD4 and CXCR4 in Des1-inhibited compared with vehicle-treated cells. These results suggest that increased cell membrane DHSM levels do not disrupt general membrane organization. The physiological implications of increased DHSM levels in specific cell types, as well as the use of Des1 inhibitors in therapy, warrant continued research.

EXPERIMENTAL PROCEDURES

Materials

Egg phosphatidylcholine (PC), egg phosphatidylethanolamine (PE), and egg diacylglycerol (DAG) were purchased from Lipid Products (South Nutfield, UK). Egg SM and Chol were from Avanti Polar Lipids (Alabaster, AL). 1,1′-Dioctadecyl-3,3,3′3′-tetramethylindocarbocyanine perchlorate (DiI) and di-ANEPPDHQ were from Invitrogen (Eugene, OR). The fluorescent probes N-(7-nitro-benz-2-oxa-1,3-diazol-4-yl)phosphatidylethanolamine (N-NBD-PE) and N-(lissamine rhodamine B sulfonyl)phosphatidylethanolamine (N-Rh-PE) were purchased from Avanti Polar Lipids (Birmingham, AL). HIV p24 ELISA from Innogenetics (Gent, Belgium), rifampicin from Boehringer (Ingelheim, Germany), Optiprep (Nycomed Pharma, Oslo, Norway); CellTiter-Glo Luminescent Cell Viability Assay, MTS, BrightGLo Luciferase System and Dual Luciferase system were from Promega (Madison, WI). The rabbit polyclonal anti-Des1 antibody was a gift of J. M. Kraveka (Medical University of South Carolina, Charleston, SC); anti-transferrin receptor (Zymed Laboratories,

San Francisco, CA), anti-β-actin (Abcam Inc., Cambridge, UK), and anti-CD4 and anti-caveolin-1 antibodies (both from Santa Cruz Biotechnology, Santa Cruz, CA). The sequence DKWASLWNWFNITNWLWYIK (HIVc or preTM), representing the pretransmembrane stretch of HIV-1 (BH10 isolate) gp41 was synthesized by solid-phase synthesis using Fmoc chemistry, as C-terminal carboxamides and purified by HPLC at the Proteomics Unit of the University Pompeu-Fabra (Barcelona, Spain). Peptide stock solutions were prepared in dimethylsulfoxide (DMSO) (spectroscopy grade) and concentrations were determined by the bicinchoninic acid microassay (Pierce, Rockford, IL).

Chemical Synthesis

N-(7-nitro-benz-2-oxa-1,3-diazol-4-yl) ceramide (NBD-Cer) was synthesized in our facilities. DHSM was obtained by hydrogenation of sphingomyelin. 6-[N-(7-nitro-2,1,3-benzoxadiazol-4-yl)amino] hexanoylsphinganine (DHCer (C6)-NBD) and GT11 were prepared as described (Munoz-Olaya et al., 2008).

GT11pyr was synthesized from the aminodiol. 8-Bromooctanic acid (11.8 mg, 0.053 mmol) dissolved in dichloromethane (DCM, 2 ml) was added to a solution of 1-ethyl-3-(3-dimethylaminopropyl)carbodiimide (10.2 mg, 0.053 mmol) and N-hydroxybenzotriazole (8.11 mg, 0.053 mmol) in DCM, and the solution was stirred (25°C, 10 min). In parallel, triethylamine (10 μl, 0.072 mmol) was added dropwise at 25°C to a solution of the cyclopropenyla-minodiol (15 mg, 0.048 mmol) in DCM (2 ml). The activated acid was added and the mixture stirred (25°C, 12 hr). The organic layer was then washed with brine and dried (MgSO$_4$), the solvent evaporated, and the residue was purified by flash chromatography. Elution with methylene chloride/methanol (40:1) afforded the bromoacyl analog of GT11 (20 mg, 0.038 mmol) with a yield of 80%.

The GT11 bromoacyl analog (20 mg, 0.038 mmol) was dissolved in toluene (2 ml) and, after addition of pyridine (2 ml), was heated at 90°C with stirring (2 hr). Solvents were removed under vacuum, and the residue was thoroughly washed with hexane and diethylether and then dissolved in methanol and filtered. Evaporation of methanol afforded GT11-pyr (15 mg, 29 mmol, 75% yield) as a white solid.

Dihydroceramide Desaturase Activity

6-[N-(7-nitro-2,1,3-benzoxadiazol-4-yl)amino] hexanoylsphinganine (DHCer-C6NBD 50 μM in ethanol), alone or with inhibitors, was incubated (3 hr, 37°C) with the cells. After cell lysis by hypotonic shock and sonication, the lysates were diluted with methanol (900 μl) and centrifuged (17,000 g, 3 min). The supernatant was analyzed by HPLC coupled to a fluorescence detector, using a reversed-phase column eluted with 20% H$_2$O and 80% acetonitrile, both with a 0.1% of trifluoroacetic acid. Fluorescence emission was recorded at 530 nm (excitation at 465 nm). A total of 100 μl was injected and each sample was run for up to 15 min.

Lipid phase Studies

The appropriate lipid mixtures in organic solvent contained 0.2 mol % DiI, 0.4 mol % NBD-Cer, or 0.1 mol % Laurdan as needed. Multilamellar (MLV), large unilamellar (LUV), and giant unilamellar (GUV) vesicles were prepared as described (Sot et al., 2008). Excitation wavelengths were 430 nm for NBD-Cer and 561 nm for DiI. Images were collected through two channels using band-pass filters of 515 ± 15 nm for NBD-Cer and 593 ± 20 nm for DiI. The generalized polarization (GP) of Laurdan 829 was measured in a SLM-AMINCO 8100 spectrofluorometer, equipped with thermoregulated cell holders. The excitation GP$_{EX}$ parameter was calculated according to

$$GP_{EX} = (I_{440} - I_{490})/(I_{440} - I_{490})$$

where I_{440} and I_{490} are the emission intensities obtained at 440 and 490 nm, respectively, exciting at 360 nm. The final probe/lipid molar ratio was 1/1000.

GUV were stained with di-4-ANEPPDHQ (10 μM) dissolved in buffer, and images analyzed in an inverted confocal fluorescence microscope with a high efficiency spectral detector (Leica TCS SP5, Leica Microsystems CMS GmbH, Mannheim, Germany). The excitation wavelength was 488 nm. Images were collected simultaneously in the 500–550 and 650–730 nm channels and analyzed with the LAS AF software (Leica Microsystems). Differential scanning calorimetry (DSC) measurements were performed on MLV as described (Sot et al., 2008).

Cell lines and Cytotoxic Assays

Human embryonic kidney (HEK)-293, HEK293CD4 (a subclone stably expressing CD4 receptor), and TZM-b1 cells were cultured as described (Mañes et al., 2000). Cell viability after 24 hr incubation with GT11 (not shown) or GT11pyr was assessed by trypan blue staining and MTS and compared with vehicle-treated cells. The cell cycle was analyzed by FACS after propidium iodide staining.

DRM Isolation

GT11pyr-incubated HEK293CD4 cells (24 hr, 37°C) were lysed and DRM isolated (Mañes et al., 2000). Five fractions were collected from the top to the bottom of the gradient, the first corresponding to the DRM fraction. Half was precipitated with TCA and analyzed by western blot with indicated antibodies, and half processed for lipid composition analysis, using UPLC coupled to an orthogonal acceleration time-of-flight mass spectrometer with an electrospray ionization interface (LCT Premier; Waters, Millford, MA). Data were acquired using positive ionization mode over a mass range of m/z 50–1500 in W-mode. A scan time of 0.15 s and interscan delay of 0.01 s were used at a nominal instrument resolution of 11500 (FWHM). Leucine enkephalin was used as the lock spray calibrant. Accurate masses used for correction were MH m/z 556.2771 and [M-H] m/z 554.2615. These conditions preclude the use of two standards flanking the mass spectrometry region of interest.

Immunofluorescence Analyses

For antibody-induced copatching, HEK293CD4 cells or HEK293 transfected with GFP-GPI (raft marker) were incubated (30 min, 12°C) with a mouse monoclonal anti-CD4 (HP2.6, Del Real et al., 2002) or anti-CXCR4 (K1046, Santa Cruz Biotechnology) antibodies, and biotinylated cholera toxin β-subunit, followed by incubation with appropriate Cy2 secondary antibodies and Cy3-streptavidin (Jackson ImmunoResearch, West Grove, PA), fixed with paraformaldehyde (3.7%, 5 min, 4°C) and methanol (5 min, −20°C), and analyzed by confocal microscopy. Images were acquired in an Olympus-F1000 confocal microscope and processed with Image J.

For gp120-induced copatching, PBMCs were sequentially incubated (30 min, 12°C) with recombinant gp120 (T cell line-adapted X4 virus, isolate IIIB, AIDS Research and Reference Reagent Program, NIAID, NIH), and a rabbit polyclonal anti-gp120 raised in our laboratory in combination with FITC-HP2.6, and biotinylated CXCR4 (FAB172, R&D Systems, Minneapolis, MN) antibodies. Finally, anti-rabbit or streptavidin-Cy5 were added (30 min, 12°C), fixed, and analyzed by confocal microscopy.

Env-Mediated Cell-Cell Fusion Assays

HEK293CD4 cells (and HEK293 cells as negative control) were transfected with pSCluc containing the firefly luciferase gene under the vaccinia virus 7.5 promoter, and pNull promoterless renilla luciferase plasmids, and then incubated with GT11 C8 (24 hr, 37°C). HIV-1env_{IIIB} was introduced into effector HEK293 cells by infection with a recombinant vaccinia virus (1 hr, 37°C); 12 hr post-infection, effector cells cultured in rifampicin (100 μg/ml) were mixed (6 hr, 37°C) with GT11-treated HEK293CD4 cells (1:2 ratio), and firefly and renilla activity quantified in cell lysates. Relative light units (RLU) were calculated as the quotient of firefly and renilla activity values, and were indicative of effector:target cell fusion.

HIV-1 Infectivity Assays

Single-round infection experiments were performed as described (Del Real et al., 2002). Replication-deficient HIV-1 viruses were generated by cotransfecting pNL4.3lucR-E- (Dr. N. Landau, AIDS Research and Reference Reagent Program, NIAID, NIH) and either ADA, NL4.3, or VSVG envelopes in HEK293T cells. Equal amounts (45 ng of p24) of replication-deficient HIV-1 viruses (HEK293T cells supernatants at 48 hr post-transfection) were added to vehicle- or GT11pyr-pretreated TZM-b1 cells (24 hr, 37°C); after 48 hr, cell infection was determined by luciferase activity measurement in cell lysates.

For infection with replication-competent HIV-1$_{NFN-SX}$ virus, TZM-bl cells (2.5 × 10^5) seeded in 96-well plates were incubated (200 μl) with GT11 (0.1–8 μM) for 24 hr or 5 days, and virus (10 ng of p24) added 24 hr later. Cells were assayed for luciferase activity 48 hr later (BrightGLo Luciferase System, Promega) in a Fluoroskan Ascent FL luminometer. Cell viability was assayed in

parallel with CellTiter-Glo Luminescent Cell Viability Assay (Promega). The percentage of inhibition was calculated as described (Buzón et al., 2008).

For knockdown experiments, TZM-bl cells were transfected with vehicle (mock), siRNA control (Ambion Silencer siRNA control; 40 nM) or Des1-specific siRNA (5′-CCUUCAAUGU GGGUUAUCAtt-3′; 40 nM) using Lipofect-amine 2000 (Invitrogen); after 4 days, cells were assayed for Des1 levels by western blot, Des1 activity, or exposed to HIV-1$_{NFN-SX}$ (2, 10, or 50 ng p24) and infectivity analyzed as above.

Intervesicular Lipid Mixing

Membrane lipid mixing was monitored in a Jobin Yvon Fluoromax-3 spectro-fluorometer using a resonance energy transfer (RET) assay. The assay is based on the dilution of N-NBD-PE and N-Rh-PE as described (Saez-Cirion et al., 2002).

SUPPLEMENTAL INFORMATION

Supplemental Information includes six figures and two tables and can be found with this article online at doi:10.1016/j.chembiol.2010.05.023.

REFERENCES

Almeida, P.F., Vaz, W.L., and Thompson, T.E. (1993). Percolation and diffusion in three-component lipid bilayers: effect of cholesterol on an equimolar mixture of two phosphatidylcholines. Biophys. J. 64, 399–412.

Bagatolli, L.A. (2006). To see or not to see: lateral organization of biological membranes and fluorescence microscopy. Biochim. Biophys. Acta 1758, 1541–1556.

Barrero-Villar, M., Cabrero, J.R., Gordon-Alonso, M., Barroso-Gonzalez, J., Alvarez-Losada, S., Munoz-Fernandez, M.A., Sanchez-Madrid, F., and Valenzuela-Fernandez, A. (2009). Moesin is required for HIV-1-induced CD4-CXCR4 interaction, F-actin redistribution, membrane fusion and viral infection in lymphocytes. J. Cell Sci. 122, 103–113.

Baumgart, T., Hammond, A.T., Sengupta, P., Hess, S.T., Holowka, D.A., Baird, B.A., and Webb, W.W. (2007). Large-scale fluid/fluid phase separation of proteins and lipids in giant plasma membrane vesicles. Proc. Natl. Acad. Sci. USA 104, 3165–3170.

Brugger, B., Graham, C., Leibrecht, I., Mombelli, E., Jen, A., Wieland, F., and Morris, R. (2004). The membrane domains occupied by glycosylphosphatidylinositol-anchored prion protein and Thy-1 differ in lipid composition. J. Biol. Chem. 279, 7530–7536.

Brugger, B., Glass, B., Haberkant, P., Leibrecht, I., Wieland, F.T., and Krausslich, H.G. (2006). The HIV lipidome: a raft with an unusual composition. Proc. Natl. Acad. Sci. USA 103, 2641–2646.

Buzón, M.J., Marfil, S., Puertas, M.C., Garcia, E., Clotet, B., Ruiz, L., Blanco, J., Martinez-Picado, J., and Cabrera, C. (2008). Raltegravir susceptibility and

fitness progression of HIV type-1 integrase in patients on long-term antiretroviral therapy. Antivir. Ther. 13, 881–893.

Byrdwell, W.C., Borchman, D., Porter, R.A., Taylor, K.G., and Yappert, M.C. (1994). Separation and characterization of the unknown phospholipid in human lens membranes. Invest. Ophthalmol. Vis. Sci. 35, 4333–4343.

Carter, G.C., Bernstone, L., Sangani, D., Bee, J.W., Harder, T., and James, W. (2009). HIV entry in macrophages is dependent on intact lipid rafts. Virology 386, 192–202.

Chiantia, S., Kahya, N., Ries, J., and Schwille, P. (2006). Effects of ceramide on liquid-ordered domains investigated by simultaneous AFM and FCS. Biophys. J. 90, 4500–4508.

Collado, M.I., Goñi, F.M., Alonso, A., and Marsh, D. (2005). Domain formation in sphingomyelin/cholesterol mixed membranes studied by spin-label electron spin resonance spectroscopy. Biochemistry 44, 4911–4918.

Cremesti, A.E., Goñi, F.M., and Kolesnick, R. (2002). Role of sphingomyelinase and ceramide in modulating rafts: do biophysical properties determine biologic outcome? FEBS Lett. 531, 47–53.

de Almeida, R.F., Borst, J., Fedorov, A., Prieto, M., and Visser, A.J. (2007). Complexity of lipid domains and rafts in giant unilamellar vesicles revealed by combining imaging and microscopic and macroscopic time-resolved fluorescence. Biophys. J. 93, 539–553.

Del Real, G., Jimenez-Baranda, S., Lacalle, R.A., Mira, E., Lucas, P., Gomez-Mouton, C., Carrera, A.C., Martinez, A.C., and Mañes, S. (2002). Blocking of HIV-1 infection by targeting CD4 to nonraft membrane domains. J. Exp. Med. 196, 293–301.

Edidin, M. (2003). The state of lipid rafts: from model membranes to cells. Annu. Rev. Biophys. Biomol. Struct. 32, 257–283.

Epand, R.M. (2003). Cholesterol in bilayers of sphingomyelin or dihydrosphingomyelin at concentrations found in ocular lens membranes. Biophys. J. 84, 3102–3110.

Finnegan, C.M., Rawat, S.S., Puri, A., Wang, J.M., Ruscetti, F.W., and Blumenthal, R. (2004). Ceramide, a target for antiretroviral therapy. Proc. Natl. Acad. Sci. USA 101, 15452–15457.

Finnegan, C.M., Rawat, S.S., Cho, E.H., Guiffre, D.L., Lockett, S., Merrill, A.H., Jr., and Blumenthal, R. (2007). Sphingomyelinase restricts the lateral diffusion of CD4 and inhibits human immunodeficiency virus fusion. J. Virol. 81, 5294–5304.

Fujita, A., Cheng, J., Hirakawa, M., Furukawa, K., Kusunoki, S., and Fujimoto, T. (2007). Gangliosides GM1 and GM3 in the living cell membrane form clusters susceptible to cholesterol depletion and chilling. Mol. Biol. Cell 18, 2112–2122.

Gallo, S.A., Finnegan, C.M., Viard, M., Raviv, Y., Dimitrov, A., Rawat, S.S., Puri, A., Durell, S., and Blumenthal, R. (2003). The HIV Env-mediated fusion reaction. Biochim. Biophys. Acta 1614, 36–50.

Gómez-Moutón, C., Abad, J.L., Mira, E., Lacalle, R.A., Gallardo, E., Jiménez-Baranda, S., Illa, I., Bernad, A., Mañes, S., and Martínez-A., C. (2001). Segregation of leading-edge and uropod components into specific lipid rafts during T cell polarization. Proc. Natl. Acad. Sci. USA 98, 9642–9647.

Goñi, F.M., and Alonso, A. (2000). Membrane fusion induced by phospholipase C and sphingomyelinases. Biosci. Rep. 20, 443–463.

Goñi, F.M., and Alonso, A. (2009). Effects of ceramide and other simple sphingolipids on membrane lateral structure. Biochim. Biophys. Acta 1788, 169–177.

Goñi, F.M., Alonso, A., Bagatolli, L.A., Brown, R.E., Marsh, D., Prieto, M., and Thewalt, J.L. (2008). Phase diagrams of lipid mixtures relevant to the study of membrane rafts. Biochim. Biophys. Acta 1781, 665–684.

Hancock, J.F. (2006). Lipid rafts: contentious only from simplistic standpoints. Nat. Rev. Mol. Cell Biol. 7, 456–462.

He, J., Choe, S., Walker, R., Di Marzio, P., Morgan, D.O., and Landau, N.R. (1995). Human immunodeficiency virus type 1 viral protein R (Vpr) arrests cells in the G2 phase of the cell cycle by inhibiting p34cdc2 activity. J. Virol. 69, 6705–6711.

Hug, P., Lin, H.M., Korte, T., Xiao, X., Dimitrov, D.S., Wang, J.M., Puri, A., and Blumenthal, R. (2000). Glycosphingolipids promote entry of a broad range of

human immunodeficiency virus type 1 isolates into cell lines expressing CD4, CXCR4, and/or CCR5. J. Virol. 74, 6377–6385.

Ipsen, J.H., Karlstrom, G., Mouritsen, O.G., Wennerstrom, H., and Zuckermann, M.J. (1987). Phase equilibria in the phosphatidylcholine-cholesterol system. Biochim. Biophys. Acta 905, 162–172.

Jacobson, K., Mouritsen, O.G., and Anderson, R.G. (2007). Lipid rafts: at a crossroad between cell biology and physics. Nat. Cell Biol. 9, 7–14.

Jimenez-Baranda, S., Gomez-Mouton, C., Rojas, A., Martinez-Prats, L., Mira, E., Lacalle, R.A., Valencia, A., Dimitrov, D.S., Viola, A., Delgado, R., et al. (2007). Filamin-A regulates actin-dependent clustering of HIV receptors. Nat. Cell Biol. 9, 838–846.

Jin, L., Millard, A.C., Wuskell, J.P., Dong, X., Wu, D., Clark, H.A., and Loew, L.M. (2006). Characterization and application of a new optical probe for membrane lipid domains. Biophys. J. 90, 2563–2575.

Jolly, C., Kashefi, K., Hollinshead, M., and Sattentau, Q. (2004). HIV-1 cell to cell transfer across an Env-induced, actin-dependent synapse. J. Exp. Med. 199, 283–293.

Kolter, T., and Sandhoff, K. (2006). Sphingolipid metabolism diseases. Biochim. Biophys. Acta 1758, 2057–2079.

Kuhmann, S.E., Platt, E.J., Kozak, S.L., and Kabat, D. (2000). Cooperation of multiple CCR5 coreceptors is required for infections by human immunodeficiency virus type 1. J. Virol. 74, 7005–7015.

Kuikka, M., Ramstedt, B., Ohvo-Rekila, H., Tuuf, J., and Slotte, J.P. (2001). Membrane properties of D-erythro-N-acyl sphingomyelins and their corresponding dihydro species. Biophys. J. 80, 2327–2337.

Kusumi, A., Koyama-Honda, I., and Suzuki, K. (2004). Molecular dynamics and interactions for creation of stimulation-induced stabilized rafts from small unstable steady-state rafts. Traffic 5, 213–230.

Liao, Z., Cimakasky, L.M., Hampton, R., Nguyen, D.H., and Hildreth, J.E. (2001). Lipid rafts and HIV pathogenesis: host membrane cholesterol is required for infection by HIV type 1. AIDS Res. Hum. Retroviruses 17, 1009–1019.

Liu, N.Q., Lossinsky, A.S., Popik, W., Li, X., Gujuluva, C., Kriederman, B., Roberts, J., Pushkarsky, T., Bukrinsky, M., Witte, M., et al. (2002). Human immunodeficiency virus type 1 enters brain microvascular endothelia by macropinocytosis dependent on lipid rafts and the mitogen-activated protein kinase signaling pathway. J. Virol. 76, 6689–6700.

Lorizate, M., Bruegger, B., Akiyama, H., Glass, B., Mueller, B., Anderluh, G., Wieland, F.T., and Krausslich, H.G. (2009). Probing HIV-1 membrane liquid order by laurdan staining reveals producer cell dependent differences. J. Biol. Chem. 284, 22238–22247.

Luzzati, V., Gulik-Krzywicki, T., Rivas, E., Reiss-Husson, F., and Rand, R.P. (1968). X-ray study of model systems. Structure of the lipid-water phases in correlation with the chemical composition of the lipids. J. Gen. Physiol. 51, 37–43.

Mabrey, S., and Sturtevant, J.M. (1976). Investigation of phase transitions of lipids and lipid mixtures by sensitivity differential scanning calorimetry. Proc. Natl. Acad. Sci. USA 73, 3862–3866.

Mañes, S., del Real, G., Lacalle, R.A., Lucas, P., Gomez-Mouton, C., Sanchez-Palomino, S., Delgado, R., Alcami, J., Mira, E., and Martinez, A.C. (2000). Membrane raft microdomains mediate lateral assemblies required for HIV-1 infection. EMBO Rep. 1, 190–196.

Mañes, S., and Viola, A. (2006). Lipid rafts in lymphocyte activation and migration. Mol. Membr. Biol. 23, 59–69.

Mañes, S., del Real, G., and Martínez-A., C. (2003). Pathogens: raft hijackers. Nat. Rev. Immunol. 3, 557–568.

Meder, D., Moreno, M.J., Verkade, P., Vaz, W.L., and Simons, K. (2006). Phase coexistence and connectivity in the apical membrane of polarized epithelial cells. Proc. Natl. Acad. Sci. USA 103, 329–334.

Megha, L.E. (2004). Ceramide selectively displaces cholesterol from ordered lipid domains (rafts): implications for lipid raft structure and function. J. Biol. Chem. 279, 9997–10004.

Mukherjee, S., and Maxfield, F.R. (2004). Membrane domains. Annu. Rev. Cell Dev. Biol. 20, 839–866.

Munoz-Olaya, J.M., Matabosch, X., Bedia, C., Egido-Gabas, M., Casas, J., Llebaria, A., Delgado, A., and Fabrias, G. (2008). Synthesis and biological activity of a novel inhibitor of dihydroceramide desaturase. ChemMedChem 3, 946–953.

Nyholm, T., Nylund, M., Soderholm, A., and Slotte, J.P. (2003a). Properties of palmitoyl phosphatidylcholine, sphingomyelin, and dihydrosphingomyelin bilayer membranes as reported by different fluorescent reporter molecules. Biophys. J. 84, 987–997.

Nyholm, T.K., Nylund, M., and Slotte, J.P. (2003b). A calorimetric study of binary mixtures of dihydrosphingomyelin and sterols, sphingomyelin, or phosphatidylcholine. Biophys. J. 84, 3138–3146.

Ollila, F., and Slotte, J.P. (2002). Partitioning of Triton X-100, deoxycholate and C(10)EO(8) into bilayers composed of native and hydrogenated egg yolk sphingomyelin. Biochim. Biophys. Acta 1564, 281–288.

Parasassi, T., De Stasio, G., d'Ubaldo, A., and Gratton, E. (1990). Phase fluctuation in phospholipid membranes revealed by Laurdan fluorescence. Biophys. J. 57, 1179–1186.

Peisajovich, S.G., Epand, R.F., Pritsker, M., Shai, Y., and Epand, R.M. (2000). The polar region consecutive to the HIV fusion peptide participates in membrane fusion. Biochemistry 39, 1826–1833.

Saez-Cirion, A., Nir, S., Lorizate, M., Agirre, A., Cruz, A., Perez-Gil, J., and Nieva, J.L. (2002). Sphingomyelin and cholesterol promote HIV-1 gp41 pre-transmembrane sequence surface aggregation and membrane restructuring. J. Biol. Chem. 277, 21776–21785.

Sharma, P., Varma, R., Sarasij, R.C., Ira, G.K., Krishnamoorthy, G., Rao, M., and Mayor, S. (2004). Nanoscale organization of multiple GPI-anchored proteins in living cell membranes. Cell 116, 577–589.

Sot, J., Bagatolli, L.A., Goñi, F.M., and Alonso, A. (2006). Detergent-resistant, ceramide-enriched domains in sphingomyelin/ceramide bilayers. Biophys. J. 90, 903–914.

Sot, J., Ibarguren, M., Busto, J.V., Montes, L.R., Goñi, F.M., and Alonso, A. (2008). Cholesterol displacement by ceramide in sphingomyelin-containing liquid-ordered domains, and generation of gel regions in giant lipidic vesicles. FEBS Lett. 582, 3230–3236.

Steffens, C.M., and Hope, T.J. (2004). Mobility of the human immunodeficiency virus (HIV) receptor CD4 and coreceptor CCR5 in living cells: implications for HIV fusion and entry events. J. Virol. 78, 9573–9578.

Taniguchi, Y., Ohba, T., Miyata, H., and Ohki, K. (2006). Rapid phase change of lipid microdomains in giant vesicles induced by conversion of sphingomyelin to ceramide. Biochim. Biophys. Acta 1758, 145–153.

Triola, G., Fabrias, G., Dragusin, M., Niederhausen, L., Broere, R., Llebaria, A., and van Echten-Deckert, G. (2004). Specificity of the dihydroceramide desaturase inhibitor N-[(1R,2S)-2-hydroxy-1-hydroxymethyl-2-(2-tridecyl-1-cyclopropenyl)ethyl]octanamide (GT11) in primary cultured cerebellar neurons. Mol. Pharmacol. 66, 1671–1678.

Viard, M., Parolini, I., Sargiacomo, M., Fecchi, K., Ramoni, C., Ablan, S., Ruscetti, F.W., Wang, J.M., and Blumenthal, R. (2002). Role of cholesterol in human immunodeficiency virus type 1 envelope protein-mediated fusion with host cells. J. Virol. 76, 11584–11595.

Zhang, Y., Li, X., Becker, K.A., and Gulbins, E. (2009). Ceramide-enriched membrane domains -structure and function. Biochim. Biophys. Acta 1788, 178–183.